Inorganic Chemistry

pubs.acs.org/IC Article

Exploiting the Reactivity of Metal Trifluoroacetates to Access Alkali−Niobium(V) Oxyfluorides

Marcos R. Imer, Regina G. Szlag, Benjamin D. E. Oreskovic, Esteban Urones-Garrote, Susana García-Martín, and Federico A. Rabuffetti*

Cite This: *Inorg. Chem.* 2024, 63, 11842−11851 Read Online

ABSTRACT: Motivated by the lack of facile routes to alkali−niobium(V) oxyfluorides KNb_2O_5F and $CsNb_2O_5F$, we investigated the reactivity of alkali trifluoroacetates $KH(tfa)_2$ and $CsH(tfa)_2$ (tfa = CF_3COO^-) toward Nb_2O_5 in the solid state. Tetragonal tungsten bronze KNb_2O_5F and pyrochlore $CsNb_2O_5F$ were obtained by simply reacting the corresponding trifluoroacetate with Nb_2O_5 at 600 °C under air, without the need for specialized containers or a controlled atmosphere. Thermolysis of $KH(tfa)_2$ in the presence of Nb_2O_5 yielded single-phase polycrystalline KNb_2O_5F. By contrast, the reaction between $CsH(tfa)_2$ and Nb_2O_5 produced a mixture of $CsNb_2O_5F$ and a new oxyfluoride of formula $CsNb_3O_7F_2$, whose crystal structure was solved using powder X-ray and electron diffraction. $CsNb_3O_7F_2$ (space group *P6/mmm*) belongs to the family of hexagonal tungsten bronzes and features an open-framework structure consisting of corner-sharing $Nb(O,F)_6$ octahedra with hexagonal channels occupied by Cs^+ ions. Isomorphous $RbNb_3O_7F_2$ was obtained upon reacting $RbH(tfa)_2$ with Nb_2O_5. Synthetic optimization enabled the preparation of $RbNb_3O_7F_2$ and $CsNb_3O_7F_2$ as single-phase polycrystalline solids at 500 °C under flowing synthetic air. Both oxyfluorides were found to be semiconductors with a band gap of ≈3.5 eV. The discovery of these two oxyfluorides highlights the importance of probing the reactivity of solids whose full potential as fluorinated precursors is yet to be realized.

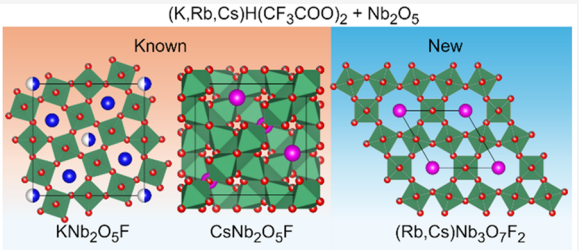

INTRODUCTION

Exploratory synthesis plays a key role in the discovery of functional materials. Typically, exploratory synthetic efforts involve the investigation of new composition spaces, the development of original synthetic methodologies, and the search for and design of novel precursors with distinct reactivity. Mixed-metal oxyfluorides containing d^0 ions from groups V and VI illustrate the significance of exploratory synthesis in materials research. These oxyfluorides feature $[MO_nF_m]$ (M = Nb^{5+}, Ta^{5+}, Mo^{6+}, W^{6+}) building blocks whose connectivity, electronic structure, and/or coordination geometry bring about functionalities such as ionic transport,[1,2] nonlinear-optical activity,[3,4] scintillation,[5] and photoluminescence.[6,7] Examples of functional oxyfluorides discovered through exploratory synthesis include (Li, Na, Rb)$SrNb_2O_6F$,[1] $KMoO_2F_3$,[4] $BaWO_2F_4$,[5] and $Cs_{10}(Nb_2O_2F_9)_3F$.[6] Synthetic efforts toward these and other compositions encompass a broad range of methodologies (e.g., solid-state reaction in metal tubes,[1,8] high-pressure/high-temperature solid-state reaction,[7] and hydrothermal[4,5]) and fluorine sources (e.g., metal fluoride salts,[1,7] fluorinated polymers,[9] aqueous HF,[4,5] and fluorine gas[10]). There is a continuous search for composition spaces, synthetic strategies, and fluorinated precursors that afford access to novel functional oxyfluorides.

For a number of years, our group has been studying the solid-state reactivity of mono- and bimetallic trifluoroacetates, especially with regard to their utility as precursors to fluoride materials. We demonstrated that solid-state thermolysis of bimetallic trifluoroacetates affords facile access to mixed-metal fluorides $AMnF_3$ (A = Na, K, Rb, Cs),[11] A'_2MnF_4 (A′ = K, Rb, Cs),[12] and $RbA''F_3$ (A″ = Mg, Ca).[13] More recently, we showed that the reactivity of monometallic trifluoroacetates may be leveraged to streamline synthetic access to alkali fluorosilicates. We reported that $KH(tfa)_2$ and $CsH(tfa)_2$ (tfa = CF_3COO^-) react with amorphous SiO_2 under air to yield hexa- and heptafluorosilicates K_2SiF_6, Cs_2SiF_6, K_3SiF_7, and Cs_3SiF_7.[14] These solids are usually synthesized via solution-phase routes that entail using aqueous HF or generating HF in situ.[15−18] A distinct advantage of metal trifluoroacetates as precursors is that they serve as both metal and fluorine sources. This is especially convenient when targeting mixed-metal fluorides because the bimetallic trifluoroacetate delivers the

Received: April 25, 2024
Accepted: May 23, 2024
Published: June 10, 2024

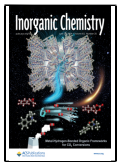

https://doi.org/10.1021/acs.inorgchem.4c01700
Inorg. Chem. 2024, 63, 11842−11851

two metals in the desired stoichiometric ratio. Moreover, the fact that trifluoromethyl groups belonging to trifluoroacetato ligands act as a fluorine source eliminates the need for external fluorinating agents. A gap in our investigation of the solid-state reactivity of metal trifluoroacetates is an evaluation of their potential as precursors to mixed-metal oxyfluoride materials. To the best of our knowledge, reports on this subject are scarce and restricted to monometallic oxyfluorides (e.g., $Ti^{IV}O_{2-0.5x}F_x$,[19] $Zr^{IV}O_xF_{4-2x}$,[19] YOF,[20] LaOF,[21] and an ill-defined barium oxyfluoride[22]). For completeness, we note that the ability of rare-earth(III) trifluoroacetates to serve as precursors for the solution-phase synthesis of oxyfluorides is well-established.[23]

In this article, we report an investigation of the reactivity of alkali trifluoroacetates $KH(tfa)_2$ and $CsH(tfa)_2$ toward Nb_2O_5, a group V refractory oxide. Our motivation was twofold. First, we aimed to streamline the solid-state synthesis of KNb_2O_5F and $CsNb_2O_5F$. Second, we sought to probe whether novel alkali−niobium(V) oxyfluorides may be accessed using trifluoroacetates as precursors. KNb_2O_5F and $CsNb_2O_5F$ were first reported by Magneli et al. in 1965 and Fourquet et al. in 1973, respectively.[24,25] Their crystal structures are shown in Figure 1. KNb_2O_5F exhibits a tetragonal tungsten bronze structure (space group *P*4/*mbm*; Figure 1a). It consists of a framework of corner-sharing $Nb(O,F)_6$ octahedra and potassium ions located in channels that extend along the *c* axis. This open-framework structure has been shown to support ionic transport.[2] On the other hand, the crystal structure of $CsNb_2O_5F$ is a cubic pyrochlore that features a much more compact arrangement of corner-sharing $Nb(O,F)_6$ octahedra (space group $Fd\bar{3}m$; Figure 1b). This arrangement may be exploited to realize red phosphors via doping with Mn^{4+}.[26] Like KNb_2O_5F, the anionic substructure of $CsNb_2O_5F$ exhibits occupational disorder of oxide and fluoride. A review of synthetic approaches to KNb_2O_5F and $CsNb_2O_5F$ reveals the absence of straightforward routes, a common occurrence in the preparation of alkali−niobium(V) and alkali−tantalum(V) oxyfluorides. Reported solid-state syntheses of KNb_2O_5F entail the solid-state reaction of $KF:Nb_2O_5$ or $KNbO_3:NbO_2F:Nb_2O_5$ mixtures in sealed platinum tubes at temperatures ranging from 850 to 1000 °C.[24,25,27] Likewise, $CsNb_2O_5F$ has been prepared by heating a $CsF:Nb_2O_5$ mixture in gold or platinum tubes at temperatures ranging from 700 to 1100 °C.[25,28,29] On this basis, we decided to revisit the solid-state synthesis of KNb_2O_5F and $CsNb_2O_5F$. The first section of this article describes our efforts toward streamlining the synthesis of these oxyfluorides using alkali trifluoroacetates and fluorides as precursors and routine experimental conditions (i.e., heating under air in alumina containers). The second section describes how the distinct reactivity of trifluoroacetates may be exploited to access new alkali−niobium(V) oxyfluorides. Specifically, it reports the discovery of a hexagonal tungsten bronze of formula $CsNb_3O_7F_2$ and of its isomorphous rubidium counterpart $RbNb_3O_7F_2$. The structural analysis process that led to elucidation of their crystal structures is described step-by-step. This process entailed coupling powder X-ray and electron diffraction and provided guidance to optimize the synthetic conditions that led to single-phase polycrystalline $CsNb_3O_7F_2$ and $RbNb_3O_7F_2$. Results presented herein highlight the significance of exploratory synthesis as a means of facilitating access to known oxyfluorides and of discovering new compositions.

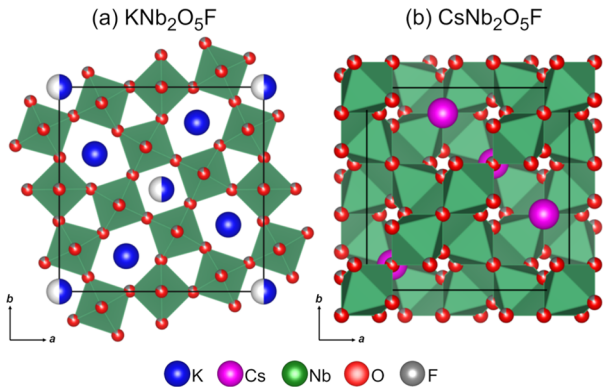

Figure 1. Crystal structures of KNb_2O_5F (a) and $CsNb_2O_5F$ (b). Unit cells are depicted with solid black lines.

■ EXPERIMENTAL SECTION

Synthesis of Alkali Trifluoroacetate Precursors. Polycrystalline $KH(tfa)_2$, $RbH(tfa)_2$, and $CsH(tfa)_2$ were synthesized via solvent evaporation under flowing nitrogen.[30] Starting reagents included K_2CO_3 (99%), Rb_2CO_3 (99.8%), Cs_2CO_3 (99.9%), and anhydrous CF_3COOH (99%) purchased from Sigma-Aldrich and used as received. Double-distilled water was used as a cosolvent. Crystallization occurred upon solvent evaporation at 65 °C for 24 h (potassium) and 48 h (rubidium and cesium). The procedure is described in detail elsewhere.[14] 2 mmol of metal trifluoroacetate were targeted per synthesis.

Synthesis of KNb_2O_5F and $CsNb_2O_5F$. KNb_2O_5F and $CsNb_2O_5F$ were synthesized via solid-state reaction under air. Starting materials included $KH(tfa)_2$ and $CsH(tfa)_2$ prepared via solvent evaporation and KF (99%), CsF (99.9%), and Nb_2O_5 (99.99%) purchased from Sigma-Aldrich and used as received. Four mixtures were prepared by mixing and grinding stoichiometric amounts of the starting materials in an agate mortar in a nitrogen-filled glovebox; these were $KH(tfa)_2:Nb_2O_5$ (≈160 mg), $CsH(tfa)_2:Nb_2O_5$ (≈150 mg), $KF:Nb_2O_5$ (≈100 mg), and $CsF:Nb_2O_5$ (≈100 mg). Reaction mixtures were transferred to 5 mL alumina crucibles, which were then covered with alumina disks, removed from the glovebox, and quickly transferred to a box furnace preheated at 100 °C. Subsequently, they were heated under air (relative humidity 25−35%) at 600 °C for 1 h using a rate of 10 °C min^{-1}. Once heating was completed, the furnace was allowed to cool to 250−275 °C, crucibles were removed, and intermediate grindings were performed under air. A total of five heating cycles were carried out. White powders were obtained.

Synthesis of $RbNb_3O_7F_2$ and $CsNb_3O_7F_2$. $RbNb_3O_7F_2$ and $CsNb_3O_7F_2$ were synthesized via solid-state reaction under flowing synthetic air (100 mL min^{-1}) in an SDT2960 TGA−DTA thermogravimetric analyzer (TA Instruments). $CsH(tfa)_2:Nb_2O_5$ (≈28 mg) and $RbH(tfa)_2:Nb_2O_5$ (≈39 mg) mixtures were prepared by mixing and grinding stoichiometric amounts of the starting materials (molar ratio 2:3) in an agate mortar in a nitrogen-filled glovebox. Reaction mixtures were transferred to 90 μL alumina crucibles, which were then covered with alumina disks, removed from the glovebox, and quickly transferred to the thermogravimetric analyzer. Therein, they were held at 35 °C for 10 min and then heated at 500 °C using a rate of 10 °C min^{-1}. Heating was stopped as soon as the set temperature was reached, and the furnace was allowed to cool to room temperature. Three additional reaction cycles were conducted in which the mixtures were heated at 500 °C for 0.5 h (cesium) or 1 h (rubidium). Intermediate grindings were performed under air. White products were thus obtained.

Powder X-ray Diffraction (PXRD). PXRD patterns were collected using a Bruker D2 Phaser diffractometer operated at 30 kV and 10 mA. Cu Kα radiation (λ = 1.5418 Å) was employed. A nickel filter was used to remove Kβ. Diffractograms were collected in

https://doi.org/10.1021/acs.inorgchem.4c01700
Inorg. Chem. 2024, 63, 11842−11851

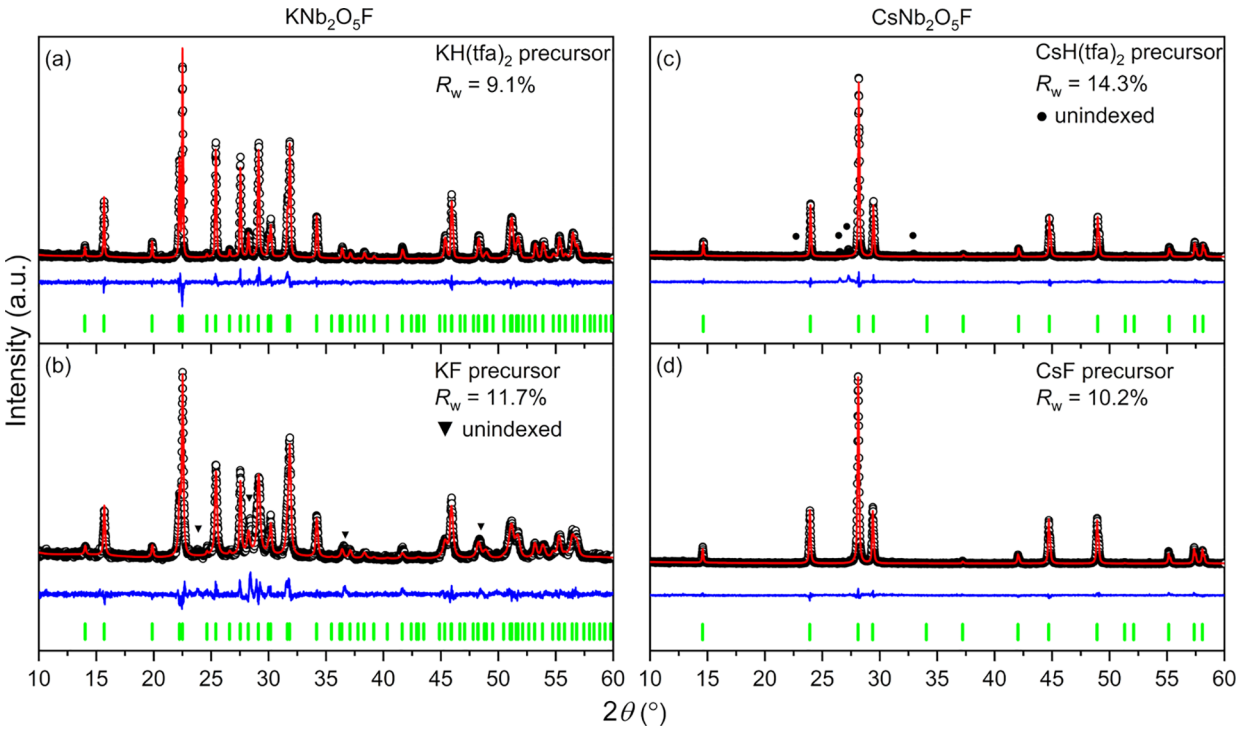

Figure 2. Rietveld analysis of the PXRD patterns of products resulting from the reaction of alkali trifluoroacetates and fluorides with Nb_2O_5. Experimental data (○), calculated pattern (solid red line), difference curve (solid blue line, offset for clarity), and tick marks corresponding to the calculated diffraction maxima (green vertical bars) are shown. Unindexed maxima in (b) and (c) are indicated with ▼ and ● symbols, respectively.

the 10−60° 2θ range using a step size of 0.012° and a step time of 0.4 s, unless otherwise noted.

Rietveld Analysis. Rietveld analyses[31,32] were carried out using the General Structure Analysis System II (GSAS-II).[33] The following parameters were refined: (1) scale factor; (2) background, which was modeled using a shifted Chebyschev polynomial function; (3) instrument parameters, including diffractometer constants and contributions to peak profile; (4) lattice constants, (5) atomic coordinates when allowed by symmetry; (6) isotropic atomic displacements parameters; (7) crystallite size and microstrain. Difference curves and R_w residuals were employed to assess the quality of the refined structural models. Crystal structures were visualized using VESTA.[34]

Crystal Structure Determination. The crystal structure of $CsNb_3O_7F_2$ was solved using EXPO2014[35] and refined using GSAS-II. Details of the structure solution procedure and rationale are provided in the Results and Discussion section.

Electron Diffraction and Microscopy. Selected area electron diffraction (SAED), convergent beam electron diffraction (CBED), and X-ray energy dispersive spectrometric (XEDS) analyses were performed using a JEM2100HT microscope (JEOL Ltd.) operating at 200 kV. Scanning transmission electron microscopy maps (STEM−XEDS) were obtained using a Talos F200X G2 S/TEM (Thermo Scientific) operating at 200 kV. Polycrystalline $CsNb_3O_7F_2$ and $RbNb_3O_7F_2$ were dispersed in toluene and drop-casted onto 200-mesh copper grids coated with a Lacey carbon film (Ted Pella Inc.).

■ RESULTS AND DISCUSSION

Section I. Synthesis of KNb_2O_5F and $CsNb_2O_5F$ Revisited. Our goal was to find out if alkali trifluoroacetates and fluorides are suitable to streamline the solid-state synthesis of KNb_2O_5F and $CsNb_2O_5F$. Moreover, we sought to pinpoint differences between the reactivity of trifluoroacetates and fluorides toward Nb_2O_5 and investigate whether they may be exploited to access previously unknown oxyfluoride phases. Mixtures consisting of the alkali metal precursor and Nb_2O_5 in a 1:1 molar ratio were heated at 600 °C for 5 h under air, that is, five cycles of 1 h each, as described in the Experimental section. Reaction progress was followed using PXRD. Results from these studies are summarized in Figure 2, where patterns of the products obtained after the fifth heating cycle are shown along with the corresponding Rietveld analyses. Patterns collected after intermediate cycles are given in Figures S1 and S2. The reaction of $KH(tfa)_2$ with Nb_2O_5 yielded phase pure KNb_2O_5F (Figure 2a). All diffraction maxima were indexed to the oxyfluoride phase (PDF No. 00-036-0808); no secondary crystalline phases were observed. KNb_2O_5F was obtained as the sole crystalline phase in the second heating cycle and remained intact during three additional heating cycles (Figure S1). Phase pure KNb_2O_5F could not be obtained using KF as the alkali metal precursor. Reaction of this metal fluoride with Nb_2O_5 yielded KNb_2O_5F as the major phase along with unindexed reflections at 2$\theta \approx$ 23.7, 28.4, 36.6, and 48.4° (Figure 2b). Heating past the second cycle did not reduce their intensity relative to the maxima belonging to the oxyfluoride phase, indicating the stability of this secondary phase at 600 °C (Figure S1). Structural parameters extracted from Rietveld analyses are given in Table 1. Occupancy factors (f) of the K1 and K2 sites were refined constrained to $2 \times f_{K1} + 4 \times f_{K2} = 5$. Isotropic displacement parameters were constrained to $U^{iso}{}_{K} = 1.2 \times U^{iso}{}_{Nb}$ and $U^{iso}{}_{O,F} = 1.5 \times U^{iso}{}_{Nb}$. Crystallochemically meaningful values were obtained for all parameters. Refined atomic coordinates were quite similar to those of the starting structural model, which is given in Table S1. Only potassium site occupancies changed noticeably upon refinement. These went from 0.5 and 1.0 for K1 and K2 in the starting model to 0.653(8) and 0.924(4), respectively, in KNb_2O_5F prepared using $KH(tfa)_2$. Likewise, occupancies equal to 0.801(13) and 0.850(6) were refined for K1 and K2, respectively, in the oxyfluoride prepared using KF as a

https://doi.org/10.1021/acs.inorgchem.4c01700
Inorg. Chem. 2024, 63, 11842−11851

Table 1. Refined Structural Parameters of KNb_2O_5F and $CsNb_2O_5F$

KNb_2O_5F ($P4/mbm$)[a]				$CsNb_2O_5F$ ($Fd\bar{3}m$)[b]			
alkali precursor		$KH(tfa)_2$	KF	alkali precursor		$CsH(tfa)_2$	CsF
a (Å)		12.6337(4)	12.6512(9)	a (Å)		10.5265(4)	10.5270(3)
c (Å)		3.94817(10)	3.9546(3)				
V (Å^3)		630.17(5)	632.96(12)	V (Å^3)		1166.41(12)	1166.59(9)
K2	x	0.1725(4)	0.1720(6)	O1, F1	x	0.3126(7)	0.3132(5)
	y	0.6725(4)	0.6720(6)				
Nb1	x	0.07314(19)	0.0733(3)				
	y	0.2144(3)	0.2170(4)				
O2, F2	x	0.1440(8)	0.1346(11)				
	y	0.0697(12)	0.0742(17)				
O3, F3	x	0.3506(10)	0.3453(15)				
	y	0.0029(6)	0.0039(8)				
O4, F4	x	0.0746(8)	0.0727(11)				
	y	0.2118(9)	0.2192(13)				
O5, F5	x	0.2854(7)	0.2690(10)				
f_{K1}		0.653(8)	0.801(13)				
f_{K2}		0.924(4)	0.850(6)				
U^{iso}_{K}[c]		2.53(10)	1.10(17)	U^{iso}_{Cs}[c]		3.76(17)	3.82(11)
U^{iso}_{Nb}[c]		2.10(9)	0.92(14)	U^{iso}_{Nb}[c]		2.48(14)	2.58(10)
$U^{iso}_{O,F}$[c]		3.16(13)	1.4(3)	$U^{iso}_{O,F}$[c]		5.6(3)	5.73(17)
R_w (%)		9.6	11.5	R_w (%)		14.3	10.3

[a]33 ($KH(tfa)_2$) and 32 (KF) parameters refined. [b]16 ($CsH(tfa)_2$) and 15 (CsF) parameters refined. [c]Given in Å^2 as 100 × U.

precursor. Potassium disorder has been shown to depend strongly on the synthesis conditions. For example, De-Yu and coworkers reported values of 0.5 (K1) and 1.0 (K2) for KNb_2O_5F synthesized from $KNbO_3$, NbO_2F, and Nb_2O_5 in sealed tubes at temperatures ranging from 850 to 1000 °C for 3−5 days.[27] An analogous reactivity study was performed for cesium. $CsH(tfa)_2$ and CsF yielded $CsNb_2O_5F$ upon reaction with Nb_2O_5 at 600 °C under air (Figure 2c,d). Structural parameters extracted for the oxyfluoride via Rietveld analysis were in line with those of the starting model (Tables 1 and S1). Isotropic displacement parameters were refined constrained to $U^{iso}_{O,F} = 1.5 \times U^{iso}_{Cs}$. Phase pure $CsNb_2O_5F$ (PDF No. 01-073-0995) could only be obtained using the metal fluoride precursor (Figure 2d). $CsNb_2O_5F$ was obtained as the sole crystalline phase in the first heating cycle and remained intact during four additional heating cycles (Figure S2). The reaction of $CsH(tfa)_2$ with Nb_2O_5 yielded $CsNb_2O_5F$ as the major phase (Figure 2c). Four additional reflections at $2\theta \approx$ 22.7, 26.6, 27.3, and 32.9° were observed after the first heating cycle, and none of them could be indexed to crystalline phases reported in the *International Centre for Diffraction Data Powder Diffraction File* database. The intensity of these reflections relative to those of $CsNb_2O_5F$ remained unchanged during the next four cycles, pointing to the formation of one or more stable crystalline secondary phases (Figure S2). Understanding the origin of these reflections is the focus of the next section of this article. Altogether, results presented in this section demonstrate that oxyfluorides KNb_2O_5F and $CsNb_2O_5F$ may be synthesized via routine solid-state reaction at 600 °C under air, without the need for specialized containers and/or stringent conditions like those employed in previous investigations.[2,24,25,27−29] As a final note, phase pure KNb_2O_5F and $CsNb_2O_5F$ were stable under atmospheric conditions, as demonstrated by the PXRD patterns collected after storing samples in air for over a month (Figure S3).

Section II. Discovery of Oxyfluorides $CsNb_3O_7F_2$ and $RbNb_3O_7F_2$. As described in the previous section, heating an equimolar mixture of $CsH(tfa)_2$ and Nb_2O_5 at 600 °C under air led to the formation of $CsNb_2O_5F$ and one or more secondary crystalline phases. This prompted us to optimize the synthetic conditions to obtain phase pure $CsNb_2O_5F$. To this end, we decided to investigate the reaction between $CsH(tfa)_2$ and Nb_2O_5 in a thermogravimetric analyzer rather than in a box furnace. Our idea was that heating the mixture under flowing synthetic air would mimic the conditions of the box furnace while at the same time allowing us to establish a crystallization temperature for each phase. Results from PXRD analyses are summarized in Figure 3. In strike contrast to what we expected, performing the reaction in a thermogravimetric analyzer favored crystallization of the unknown phase(s) rather than yielding phase pure $CsNb_2O_5F$ (Figure 3a). The positions of the four major peaks of the unknown phase(s) ($2\theta \approx$ 22.7, 26.6, 27.3, and 32.9°) matched those observed in the pattern of the product obtained in the box furnace (Figure 3b), suggesting that they likely belong to the same crystalline phase. We then focused our synthetic efforts on isolating this new phase. To this end, experiments involving different temperature programs were conducted in a thermogravimetric analyzer. In the course of these experiments, we observed that crystallization of the $CsNb_2O_5F$ pyrochlore was hindered when the reaction mixture was heated to 600 °C and naturally cooled to room temperature once that temperature was reached (i.e., no dwelling time). The diffraction pattern of the product obtained using that temperature program featured strong maxima belonging to the unknown phase and three additional weak reflections in the $2\theta \approx$ 23−25° region (Figure 3c). As will be shown later in this article, further synthetic optimization led to the disappearance of those weak reflections, enabling the preparation of a single-phase sample. Key to that optimization process was establishing the crystal structure of the unknown phase.

The structure of the new phase was solved using a combination of powder X-ray and electron diffraction and microscopy. This process entailed the following three steps: (i)

https://doi.org/10.1021/acs.inorgchem.4c01700
Inorg. Chem. 2024, 63, 11842−11851

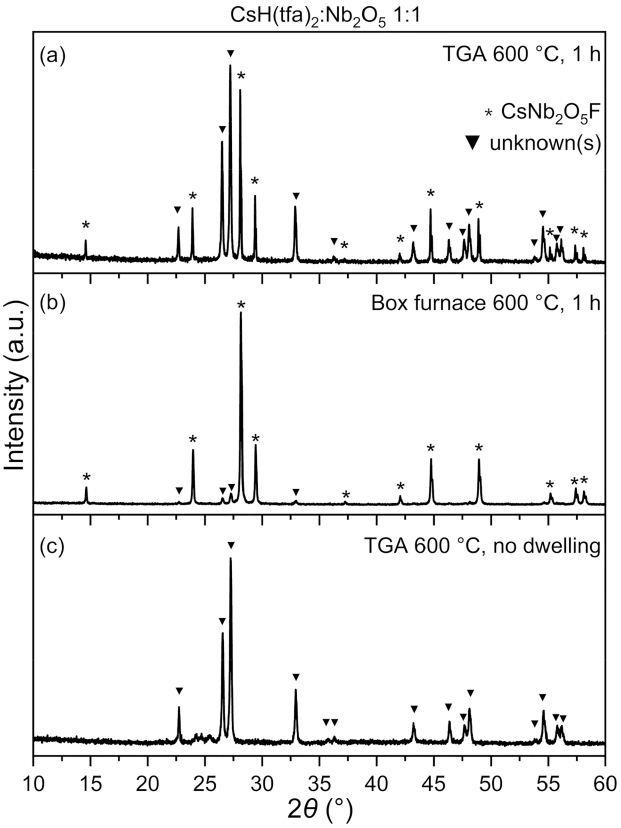

Figure 3. PXRD patterns of products resulting from heating a $CsH(tfa)_2$:Nb_2O_5 equimolar mixture at 600 °C for 1 h in a thermogravimetric analyzer (a) and a box furnace (b). The pattern of the product obtained upon reaction in a thermogravimetric analyzer with no dwelling time is given in (c). Maxima belonging to $CsNb_2O_5F$ and unknown phases are depicted with * and ▼ symbols, respectively.

use PXRD data to obtain a tentative initial structural model; (ii) use SAED and CBED to further distill this model, particularly with regard to the unit cell lattice constants and space group; and (iii) obtain a fully refined model via Rietveld analysis of the PXRD data. To begin, we recollected a diffraction pattern of the product obtained upon heating an equimolar mixture of $CsH(tfa)_2$ and Nb_2O_5 at 600 °C under synthetic flowing air in a thermogravimetric analyzer. The new pattern is shown in Figure 4a and was collected over an extended 2θ range (10−80°) and with higher counting statistics (1 s per step). A total of 15 reflections from this pattern were used for determining the unit cell. Indexing was carried out using N-TREOR09 and DICVOL06 routines included in EXPO2014.[36−38] Both routines yielded a hexagonal unit cell with lattice constants a = 7.5630 Å and c = 3.9185 Å (V = 194.4 Å^3) as the most likely option. A list of alternative unit cells and their corresponding figures of merit is given in Table S2. With the tentative unit cell in hand, we proceeded to run the space group determination routine in EXPO2014,[39−41] which yielded a total of 16 groups as the most probable options (Table S3). We selected the highest symmetry space group from this set, which was $P6/mmm$ (No. 191). This choice was made to prevent an artificial low-symmetry solution. Structure solution was then attempted using direct methods, as embedded in EXPO2014. Based on the stoichiometry of the reaction mixture, our first guess was that the new phase was a polymorph of $CsNb_2O_5F$. However,

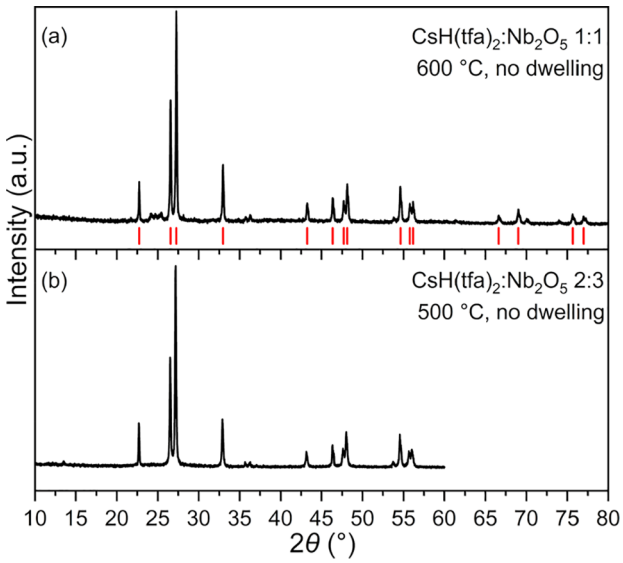

Figure 4. (a) PXRD pattern used for indexing the unit cell of the unknown phase obtained upon heating a $CsH(tfa)_2$:Nb_2O_5 equimolar mixture at 600 °C. Reflections used for indexing are depicted with red vertical bars. (b) PXRD pattern of the product obtained upon tuning the $CsH(tfa)_2$:Nb_2O_5 molar ratio to 2:3 and carrying out the reaction at 500 °C. Reactions were performed under flowing synthetic air in a thermogravimetric analyzer.

using $CsNb_2O_5F$ as the unit cell content of the starting model (Z = 1; 21.6 Å^3 per atom) led to a structure that contained cesium and oxygen but no niobium. Moreover, the resulting ionic charges were chemically meaningless. This result prompted us to examine more carefully the potential stoichiometry of the new phase. We conducted a search for isostructural materials in the *Inorganic Crystal Structure Database* using unit cell constants and symmetry as matching criteria. The search retrieved the hexagonal tungsten bronze $Rb(Nb_{1/3}W_{2/3})_3O_9$ (ICSD No. 120989).[42] This finding led us to hypothesize that the new phase featured a Cs:Nb molar ratio equal to 1:3. Attempting structure solution using $CsNb_3O_9$ as the unit cell content and space group $P6/mmm$ led to convergence, indicating that the electron density of the new phase was compatible with that of hexagonal bronzes (Table S4 and Figure S4). However, the lack of chemical meaning of the $Cs^{III}Nb_3O_9$ formula led us to consider the possibility that this new hexagonal bronze was an oxyfluoride in which O^{2-} was partially replaced by F^-; the presence of fluorine was later confirmed by elemental mapping (vide infra). On this basis, we envisioned $CsNb_3O_7F_2$ (Z = 1; 14.9 Å^3 per atom) as a hypothetical formula for the new phase. This formula was derived assuming a Cs:Nb ratio equal to 1:3 (later confirmed by XEDS, vide infra) and distributing O^{2-} and F^- ions in the nine anionic sites of the structure. The O:F ratio had to be set equal to 7:2 to ensure electroneutrality. To test this hypothesis, we prepared a mixture of $CsH(tfa)_2$ and Nb_2O_5 in a 2:3 molar ratio to match the 1:3 Cs:Nb nominal ratio in the target oxyfluoride $CsNb_3O_7F_2$. This mixture was heated at temperatures ranging from 450 to 600 °C under flowing synthetic air in a thermogravimetric analyzer, with no dwelling time. As shown in Figure 4b, reacting the optimized reaction mixture at 500 °C enabled the preparation of a sample whose survey scan (10−60°) did not show the reflections in the $2\theta \approx$ 23−25° region; further heating at that temperature had no effect other than slightly improving crystallinity (Figure

https://doi.org/10.1021/acs.inorgchem.4c01700
Inorg. Chem. 2024, 63, 11842−11851

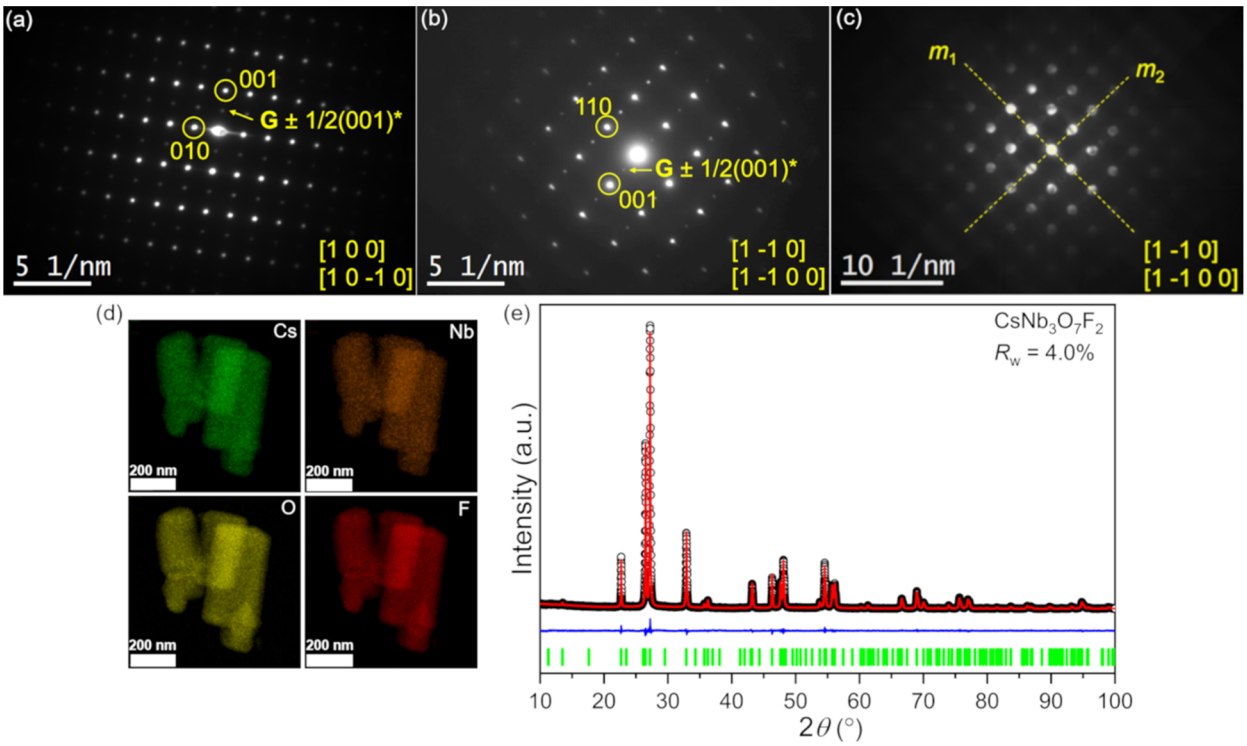

Figure 5. Electron diffraction and microscopy and X-ray diffraction analyses of $CsNb_3O_7F_2$. (a) and (b) SAED and (c) CBED patterns. Reflections used for unit cell determination are labeled in (a) and (b). Mirror planes are depicted with dashed lines in (c). (d) STEM−XEDS elemental maps. (e) Rietveld analysis of the PXRD pattern. Experimental data (○), calculated pattern (solid red line), difference curve (solid blue line, offset for clarity), and tick marks corresponding to the calculated diffraction maxima (green vertical bars) are shown. The pattern was collected with a step size and time of 0.01° and 5 s, respectively.

S5). We interpreted this result as a confirmation of the proposed 1:3 Cs:Nb molar ratio. On the other hand, the proposed hexagonal unit cell with lattice constants a = 7.5630 Å and c = 3.9185 Å failed to index *all* diffraction maxima. Although most reflections were indexed, a series of extremely weak reflections at 37.0, 38.1, 42.0, and 62.9° could not be accounted for (Figure S6). Altogether, these results demonstrated that, even though our initial structural model featured the correct stoichiometry, the unit cell lattice constants and/or symmetry had to be revised.

On this basis, we sought to establish unit cell parameters and symmetry using a different experimental probe. Electron diffraction and microscopy studies were carried out on a sample synthesized as described in the Experimental section, i.e., a $CsH(tfa)_2$:Nb_2O_5 mixture (2:3 molar ratio) heated at 500 °C for a total of 1.5 h under flowing synthetic air in a thermogravimetric analyzer. Results from these studies are summarized in Figure 5. They confirmed the hexagonal centrosymmetric space group but provided new insight into the unit cell lattice constants. SAED patterns along the $[10\bar{1}0]$ and $[1\bar{1}00]$ zone axes were indexed according to a hexagonal unit cell with lattice parameters a = 7.5630 Å and c = 3.9185 Å. Interestingly, weak extra reflections at **G** ± 1/2(001)* were observed in the patterns (Figure 5a,b), indicating that the actual value of the c lattice parameter was twice that of our initial structural model. This led us to propose a new unit cell with dimensions a = 7.5686 Å and c = 7.8370 Å (V = 388.8 Å^3; Z = 2; 15.0 Å^3 per atom), which successfully explained *all* reflections observed in the PXRD pattern of the product (Figure S7). The CBED pattern of a $CsNb_3O_7F_2$ crystal along the $[1\bar{1}00]$ zone axis exhibited 2*mm* symmetry, compatible with the centrosymmetric *P*6/*mmm* space group (Figure 5c).[43] With regard to the chemical composition, XEDS analysis of more than 20 crystals yielded a 1:3 molar ratio of Cs:Nb, consistent with the chemical formula $CsNb_3O_7F_2$. STEM−XEDS elemental mapping confirmed the incorporation of fluorine in the crystal lattice and a homogeneous distribution of all elements throughout the crystals (Figure 5d). Electron diffraction results were used to build a structural model that was subsequently refined via Rietveld analysis of an extended 2θ range PXRD pattern (10−100°, Figure 5e). Structural parameters of the starting and refined models are given in Table 2. Refined bond distances and angles are given in Table S5. Three isotropic atomic displacement parameters were refined unconstrained (U^{iso}_{Cs}, U^{iso}_{Nb}, and $U^{iso}_{O,F}$). Occupation factors of the oxygen/fluorine sites were fixed. An excellent fit was obtained as illustrated by both the flat difference curve and the low value of the fit residual (R_w = 4.0%), supporting the proposed chemical formula and hexagonal bronze structure of $CsNb_3O_7F_2$. Noteworthy is the fact that attempts to obtain *phase pure* $CsNb_3O_7F_2$ outside the thermogravimetric analyzer were unsuccessful. Although the bronze formed, products obtained by heating a $CsH(tfa)_2$:Nb_2O_5 mixture (2:3 molar ratio) in a box or tube furnace in the 500−600 °C range invariably contained $CsNb_2O_5F$. The coexistence of hexagonal bronze and pyrochlore phases was also observed by McNulty and coworkers in their study of $CsNbW_2O_9$.[44] Control experiments were carried out using CsF as the alkali metal precursor. $CsNb_2O_5F$ and unreacted Nb_2O_5 were obtained as products upon heating a CsF:Nb_2O_5 mixture (2:3 molar ratio) in the same experimental conditions in which single-phase $CsNb_3O_7F_2$ had been prepared (Figure S8). Thus, we

https://doi.org/10.1021/acs.inorgchem.4c01700
Inorg. Chem. 2024, 63, 11842−11851

Table 2. Starting and Refined Structural Parameters of $CsNb_3O_7F_2$ (*P6/mmm*)

		starting		refined[a]
a (Å)		7.5686		7.56206(10)
c (Å)		7.8370		7.83407(6)
V (Å^3)		388.324		387.970(8)
Cs1 (1*a*)[b]	*x, y, z*		0, 0, 0	
	f_{Cs1}		1	
Cs2 (1*b*)	*x, y, z*		0, 0, 0.5	
	f_{Cs2}		1	
Nb1 (6*i*)	*x, y, z*	0.5, 0, 0.25		0.5, 0, 0.2521(3)
	f_{Nb1}		1	
O1, F1 (3*f*)	*x, y, z*		0.5, 0, 0	
	$f_{O1,F1}$		0.7778, 0.2222	
O2, F2 (3*g*)	*x, y, z*		0.5, 0, 0.5	
	$f_{O2,F2}$		0.7778, 0.2222	
O3, F3 (12*o*)	*x, y,*[c] *z*	0.4192, 0.2960, 0.25		0.4205(3), 0.21024(14), 0.2361(7)
	$f_{O3,F3}$		0.7778, 0.2222	
U^{iso}_{Cs}[d]		3.22		3.17(3)
U^{iso}_{Nb}[d]		2.13		2.285(19)
$U^{iso}_{O,F}$[d]		1.27		2.34(7)
R_w (%)				4.0

[a]30 parameters refined. [b]Wyckoff positions are given in parentheses. [c]$y = x/2$. [d]Given in Å^2 as $100 \times U$.

conclude that an intrinsic reactivity difference between $CsH(tfa)_2$ and CsF—perhaps due to reactive fluorinated volatiles arising from decomposition of the trifluoroacetato moieties (e.g., CF_2)[14,45−48]—and the microenvironment within the thermogravimetric analyzer helped in achieving single-phase polycrystalline $CsNb_3O_7F_2$.

The refined crystal structure of $CsNb_3O_7F_2$ is shown in Figure 6. The structure features a framework of corner-sharing $Nb(O,F)_6$ octahedra that give rise to hexagonal channels running parallel to the *c* axis (Figure 6a). Cs^+ ions are located within these channels, and the Cs−Cs distances equal 3.917 Å.

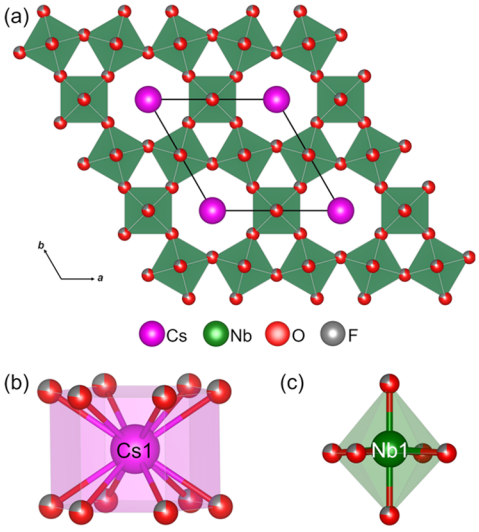

Figure 6. Refined crystal structure of $CsNb_3O_7F_2$. (a) Polyhedral view showing hexagonal channels parallel to the *c* axis. The unit cell is depicted with solid black lines. (b) and (c) Coordination environments of Cs^+ and Nb^{5+} ions.

The arrangement is similar to that observed in the $Pb_xM^V(O,F)_{3+x/2}$ bronze (M = Nb, Ta).[49] Cs^+ ions are coordinated by 12 ligands in a regular hexagonal prismatic geometry (Figure 6b). Cs−O/F bond distances equal to 3.317 and 3.444 Å are observed for the two cesium sites in the structure, respectively. Niobium adopts a distorted octahedral geometry due to a second-order Jahn−Teller distortion (Figure 6c). Nb−O/F bond distances are distributed in a 4 + 1 + 1 pattern ($Nb-O/F_{equatorial}$ = 1.965 Å; $Nb-O/F_{axial}$ = 1.942 and 1.975 Å). Nb^{5+} is displaced ≈0.017 Å along the [001] direction from the center of the $Nb(O,F)_6$ octahedron. $CsNb_3O_7F_2$ is a semiconductor with a band gap of ≈3.5 eV, as estimated from diffuse-reflectance measurements (Figure S9).

Putting the structure solution process into perspective, we observed that coming across $Rb(Nb_{1/3}W_{2/3})_3O_9$ was key to make an educated guess of the stoichiometry of the new phase. We further exploited this finding to attempt the synthesis of $RbNb_3O_7F_2$. Synthetic conditions are described in the Experimental section, i.e., a $RbH(tfa)_2$:Nb_2O_5 mixture (2:3 molar ratio) heated at 500 °C for a total of 3 h under flowing synthetic air in a thermogravimetric analyzer. Compositional XEDS and structural analyses confirmed the formation of a new oxyfluoride of formula $RbNb_3O_7F_2$, isomorphous to $CsNb_3O_7F_2$. Results from these analyses are summarized in Figure 7. SAED patterns confirmed the hexagonal unit cell (Figure 7a,b). Similar to what was observed in $CsNb_3O_7F_2$, weak extra reflections at **G** ± 1/2(001)* indicated that the actual value of the *c* lattice constant was twice that estimated from X-ray diffraction (*c* = 3.8795 Å; Figure S10). A unit cell with dimensions *a* = 7.5289 Å and *c* = 7.75917 Å (*V* = 380.9 Å^3; *Z* = 2; 14.7 Å^3 per atom) successfully explained *all* reflections observed in the PXRD pattern of the product (Figure S11). The CBED pattern of a $RbNb_3O_7F_2$ crystal along the [$1\bar{1}00$] zone axis showed 2*mm* symmetry, compatible with centrosymmetric space group *P6/mmm* (Figure 7c).[43] XEDS analysis of more than 20 crystals yielded a 1:3 molar ratio of Rb:Nb, consistent with the chemical formula $RbNb_3O_7F_2$. STEM−XEDS elemental mapping confirmed that the solid was an oxyfluoride and a homogeneous distribution of all elements throughout the crystals (Figure 7d). The hexagonal bronze structural model was fit to the PXRD data via Rietveld analysis (Figure 7e). Refined structural parameters are given in Table 3. Refined bond distances and angles are given in Table S6. Three isotropic atomic displacement parameters were refined unconstrained (U^{iso}_{Rb}, U^{iso}_{Nb}, and $U^{iso}_{O,F}$), and occupation factors of the oxygen/fluorine sites were fixed. A very good fit was obtained, as shown by both the difference curve and the low value of the fit residual (R_w = 5.5%), giving further support to the proposed chemical formula and hexagonal bronze structure of $RbNb_3O_7F_2$. Inspection of the bond distances revealed that the magnitude of Nb^{5+} off-centering is more pronounced than in $CsNb_3O_7F_2$ (0.024 vs 0.017 Å). The band gap estimated from diffuse-reflectance measurements is ≈3.5 eV, as in $CsNb_3O_7F_2$ (Figure S12). Similar to what was done for $CsNb_3O_7F_2$, control experiments were carried out using RbF as the alkali metal precursor. $RbNb_2O_5F$ and unreacted Nb_2O_5 were obtained upon heating a RbF:Nb_2O_5 mixture (2:3 molar ratio) in the same experimental conditions in which single-phase $RbNb_3O_7F_2$ had been prepared (Figure S13). This result further highlights the distinct reactivity of alkali trifluoroacetates relative to their fluoride counterparts.

https://doi.org/10.1021/acs.inorgchem.4c01700
Inorg. Chem. 2024, 63, 11842−11851

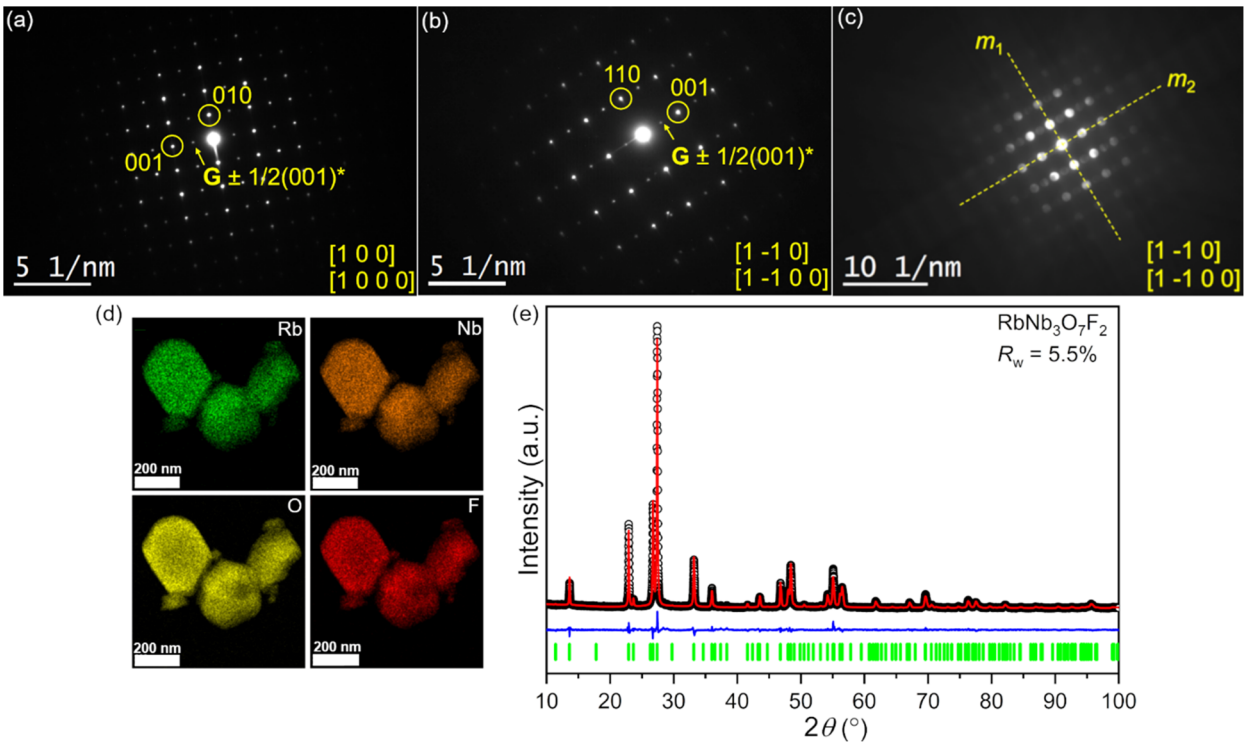

Figure 7. Electron diffraction and microscopy and X-ray diffraction analyses of $RbNb_3O_7F_2$. (a) and (b) SAED and (c) CBED patterns. Reflections used for the unit cell determination are labeled in (a) and (b). Mirror planes are depicted with dashed lines in (c). (d) STEM−XEDS elemental maps. (e) Rietveld analysis of the PXRD pattern. Experimental data (○), calculated pattern (solid red line), difference curve (solid blue line, offset for clarity), and tick marks corresponding to the calculated diffraction maxima (green vertical bars) are shown. The pattern was collected with a step size and time of 0.01° and 5 s, respectively.

Table 3. Refined Structural Parameters of $RbNb_3O_7F_2$ (*P6/mmm*)[a]

a (Å)		7.5192(2)
c (Å)		7.76332(12)
V (Å^3)		380.122(16)
Nb1 (6i)[b]	*z*	0.2530(4)
O3/F3 (12o)	*x*, *y*,[c] *z*	0.4169(3), 0.20846(14), 0.2333(9)
U^{iso}_{Rb}[d]		6.93(7)
U^{iso}_{Nb}[d]		2.28(3)
$U^{iso}_{O,F}$[d]		3.62(9)
R_w (%)		5.5

[a]31 refined parameters. [b]Wyckoff positions are given in parentheses. [c]$y = x/2$. [d]Given in Å^2 as $100 \times U$.

■ CONCLUSIONS

The reactivity of alkali trifluoroacetates $KH(tfa)_2$ and $CsH(tfa)_2$ toward Nb_2O_5 was studied in the solid state and exploited to access known and novel mixed-metal oxyfluorides. A straightforward route to KNb_2O_5F and $CsNb_2O_5F$ was demonstrated by reacting the corresponding alkali trifluoroacetate or fluoride with Nb_2O_5 under air, without the need for specialized reaction vessels and/or a controlled atmosphere. Two new hexagonal tungsten bronzes of formulas $RbNb_3O_7F_2$ and $CsNb_3O_7F_2$ were prepared by reacting a stoichiometric mixture of the corresponding alkali trifluoroacetate and Nb_2O_5 at 500 °C under flowing synthetic air in a thermogravimetric analyzer. Control experiments highlighted the distinct reactivity of alkali trifluoroacetates because $RbNb_3O_7F_2$ and $CsNb_3O_7F_2$ could not be crystallized using alkali fluoride precursors. Altogether, results reported herein enlarge the toolbox of synthetic approaches to alkali−niobium(V) oxyfluorides and expand the composition space of these mixed-anion materials. Moreover, they underscore the significance of exploring new fluorinated precursors and establishing their reactivity patterns. From a methodological standpoint, this article illustrates how combining powder X-ray and electron diffraction may be used for the quantitative structure solution of unknown phases.

Due to the limitations of using X-ray diffraction to characterize the structure of oxyfluorides, room exists for improving the structural description of $RbNb_3O_7F_2$ and $CsNb_3O_7F_2$ with regard to the anionic substructure (i.e., oxide/fluoride local ordering) and to the spatial distribution of alkali ions in the hexagonal channels (i.e., positional disorder). Although our X-ray data did not reveal displacement of these ions from their ideal positions, such displacements have been reported in several hexagonal tungsten bronzes.[49−51] Further research is needed to address these two aspects.

■ ASSOCIATED CONTENT

Supporting Information

The Supporting Information is available free of charge at https://pubs.acs.org/doi/10.1021/acs.inorgchem.4c01700.

Additional details of the synthesis of KNb_2O_5F and $CsNb_2O_5F$, additional details of the structure solution of $CsNb_3O_7F_2$ and $RbNb_3O_7F_2$, diffuse-reflectance spectra, and control experiments for $CsNb_3O_7F_2$ and $RbNb_3O_7F_2$ (PDF)

https://doi.org/10.1021/acs.inorgchem.4c01700
Inorg. Chem. 2024, 63, 11842−11851

AUTHOR INFORMATION

Corresponding Author

Federico A. Rabuffetti − *Department of Chemistry, Wayne State University, Detroit, Michigan 48202, United States;* orcid.org/0000-0001-8500-3427; Email: far@chem.wayne.edu

Authors

Marcos R. Imer − *Department of Chemistry, Wayne State University, Detroit, Michigan 48202, United States;* orcid.org/0000-0002-5907-9927

Regina G. Szlag − *Department of Chemistry, Wayne State University, Detroit, Michigan 48202, United States*

Benjamin D. E. Oreskovic − *Department of Chemistry, Wayne State University, Detroit, Michigan 48202, United States;* orcid.org/0000-0001-9583-7265

Esteban Urones-Garrote − *Departamento de Química Inorgánica, Facultad de Ciencias Químicas and Centro Nacional de Microscopía Electrónica, Universidad Complutense de Madrid, Madrid 28040, Spain;* orcid.org/0000-0002-4745-2755

Susana García-Martín − *Departamento de Química Inorgánica, Facultad de Ciencias Químicas, Universidad Complutense de Madrid, Madrid 28040, Spain;* orcid.org/0000-0003-0729-4892

Complete contact information is available at: https://pubs.acs.org/10.1021/acs.inorgchem.4c01700

Notes

The authors declare no competing financial interest.

ACKNOWLEDGMENTS

M.R.I. acknowledges the support of Wayne State University through a Thomas C. Rumble Graduate Fellowship and of the International Centre for Diffraction Data for a Ludo Frevel Scholarship. R.G.S. was partially funded through a National Science Foundation Award (DMR-2003118). S.G.-M. and E.U.-G. acknowledge the Spanish MCIN/AEI/10.13039/501100011033 for funding Project PID2022-139039OB-C22. This work used the X-ray diffraction and Electron Microscopy cores in the Lumigen Instrument Center of Wayne State University (National Science Foundation Grants MRI-1427926 and MRI-2018587). The authors thank Nishani Manamperi for her assistance with the synthesis of $RbH(tfa)_2$ and STEM elemental mapping, and Professor Leopoldo Suescun (UdelaR, Uruguay) for helpful discussions.

REFERENCES

(1) Choy, J.-H.; Kim, J.-Y.; Kim, S.-J.; Sohn, J.-S.; Han, O. H. New Dion−Jacobson-Type Layered Perovskite Oxyfluorides, $ASrNb_2O_6F$ (A = Li, Na, and Rb). *Chem. Mater.* **2001**, *13*, 906−912.

(2) Han, Y.; Yang, M.; Zhang, Y.; Xie, J.; Yin, D.; Li, C. Tetragonal Tungsten Bronze Framework as Potential Anode for Na-Ion Batteries. *Chem. Mater.* **2016**, *28*, 3139−3147.

(3) Huang, J.; Guo, S.; Zhang, Z.; Yang, Z.; Pan, S. Designing Excellent Mid-Infrared Nonlinear Optical Materials with Fluorooxo-Functional Group of d^0 Transition Metal Oxyfluorides. *Science China Materials* **2019**, *62*, 1798−1806.

(4) Hancock, J. C.; Nisbet, M. L.; Zhang, W.; Halasyamani, P. S.; Poeppelmeier, K. R. Periodic Tendril Perversion and Helices in the $AMoO_2F_3$ (A = K, Rb, NH_4, Tl) Family. *J. Am. Chem. Soc.* **2020**, *142*, 6375−6380.

(5) Ayer, G. B.; Klepov, V. V.; Smith, M. D.; Hu, M.; Yang, Z.; Martin, C. R.; Morrison, G.; zur Loye, H.-C. BaWO2F4: A Mixed Anion X-ray Scintillator with Excellent Photoluminescence Quantum Efficiency. *Dalton Transactions* **2020**, *49*, 10734−10739.

(6) Ayer, G. B.; Morrison, G.; Smith, M. D.; Jacobsohn, L. G.; zur Loye, H.-C. Luminescence and Scintillation of $[Nb_2O_2F_9]^{3-}$-Dimer-Containing Oxide−Fluorides: $Cs_{10}(Nb_2O_2F_9)_3F$, $Cs_{9.4}K_{0.6}(Nb_2O_2F_9)_3F$, and $Cs_{10}(Nb_2O_2F_9)_3Cl$. *Inorg. Chem.* **2022**, *61*, 3256−3262.

(7) Zimmerhofer, F.; Seibald, M.; Stoll, C.; Baumann, D.; Wurst, K.; Huppertz, H. Crystal Structure, Characterization, and Luminescence Properties of Mn^{4+}-Doped $K_3Nb_2O_4F_5$. *Eur. J. Inorg. Chem.* **2023**, *26*, e202200714.

(8) Kaskel, S.; Strähle, J. Synthese und Struktur von $Li_2Ta_2O_3F_6$. *Zeitschrift für anorganische und allgemeine Chemie* **1997**, *623*, 456−460.

(9) Hirai, D.; Sawai, O.; Nunoura, T.; Hiroi, Z. Facile Synthetic Route to Transition Metal Oxyfluorides via Reactions Between Metal Oxides and PTFE. *J. Fluorine Chem.* **2018**, *209*, 43−48.

(10) Thapaliya, B. P.; Self, E. C.; Jafta, C. J.; Borisevich, A. Y.; Meyer, H. M., III; Bridges, C. A.; Nanda, J.; Dai, S. Synthesizing High-Capacity Oxyfluoride Conversion Anodes by Direct Fluorination of Molybdenum Dioxide (MoO_2). *ChemSusChem* **2020**, *13*, 3825−3834.

(11) Dhanapala, B. D.; Munasinghe, H. N.; Suescun, L.; Rabuffetti, F. A. Bimetallic Trifluoroacetates as Single-Source Precursors for Alkali−Manganese Fluoroperovskites. *Inorg. Chem.* **2017**, *56*, 13311−13320.

(12) Munasinghe, H. N.; Suescun, L.; Dhanapala, B. D.; Rabuffetti, F. A. Bimetallic Trifluoroacetates as Precursors to Layered Perovskites A_2MnF_4 (A = K, Rb, and Cs). *Inorg. Chem.* **2020**, *59*, 17268−17275.

(13) Szlag, R. G.; Suescun, L.; Dhanapala, B. D.; Rabuffetti, F. A. Rubidium−Alkaline-Earth Trifluoroacetate Hybrids as Self-Fluorinating Single-Source Precursors to Mixed-Metal Fluorides. *Inorg. Chem.* **2019**, *58*, 3041−3049.

(14) Munasinghe, H. N.; Imer, M. R.; Szlag, R. G.; Suescun, L.; Rabuffetti, F. A. Reactivity of Bi- and Monometallic Trifluoroacetates Towards Amorphous SiO_2. *Dalton Transactions* **2022**, *51*, 18224−18233.

(15) Huang, L.; Zhu, Y.; Zhang, X.; Zou, R.; Pan, F.; Wang, J.; Wu, M. HF-Free Hydrothermal Route for Synthesis of Highly Efficient Narrow-Band Red Emitting Phosphor $K_2Si_{1-x}F_6{:}xMn^{4+}$ for Warm White Light-Emitting Diodes. *Chem. Mater.* **2016**, *28*, 1495−1502.

(16) Hou, Z.; Tang, X.; Luo, X.; Zhou, T.; Zhang, L.; Xie, R.-J. A Green Synthetic Route to the Highly Efficient $K_2SiF_6{:}Mn^{4+}$ Narrow-Band Red Phosphor for Warm White Light-Emitting Diodes. *Journal of Materials Chemistry C* **2018**, *6*, 2741−2746.

(17) Luo, X.; Hou, Z.; Zhou, T.; Xie, R.-J. A Universal HF-Free Synthetic Method to Highly Efficient Narrow-Band Red-Emitting $A_2XF_6{:}Mn^{4+}$ (A = K, Na, Rb, Cs; X = Si, Ge, Ti) Phosphors. *J. Am. Ceram. Soc.* **2020**, *103*, 1018−1026.

(18) Kim, Y. H.; Ha, J.; Im, W. B. Towards Green Synthesis of Mn^{4+}-Doped Fluoride Phosphors: A Review. *Journal of Materials Research and Technology* **2021**, *11*, 181−195.

(19) Rüssel, C. A Pyrolytic Route to Fluoride Glasses. I. Preparation and Thermal Decomposition of Metal Trifluoroacetates. *J. Non-Cryst. Solids* **1993**, *152*, 161−166.

(20) Saeed, N. A. M.; Coetsee, E.; Swart, H. C. Photoluminescence Studies of a YOF Phosphor Synthesized by the Pyrolysis Method. *Opt. Mater.* **2019**, *96*, 109331.

(21) Rodrigues, E. M.; Souza, E. R.; Monteiro, J. H. S. K.; Gaspar, R. D. L.; Mazali, I. O.; Sigoli, F. A. Non-Stabilized Europium-Doped Lanthanum Oxyfluoride and Fluoride Nanoparticles Well Dispersed in Thin Silica Films. *J. Mater. Chem.* **2012**, *22*, 24109−24123.

(22) Gàzquez, J.; Sandiumenge, F.; Coll, M.; Pomar, A.; Mestres, N.; Puig, T.; Obradors, X.; Kihn, Y.; Casanove, M. J.; Ballesteros, C. Precursor Evolution and Nucleation Mechanism of $YBa_2Cu_3O_x$ Films by TFA Metal−Organic Decomposition. *Chem. Mater.* **2006**, *18*, 6211−6219.

(23) Du, Y.-P.; Zhang, Y.-W.; Sun, L.-D.; Yan, C.-H. Luminescent Monodisperse Nanocrystals of Lanthanide Oxyfluorides Synthesized from Trifluoroacetate Precursors in High-Boiling Solvents. *J. Phys. Chem. C* **2008**, *112*, 405−415.

(24) Magneli, A.; Nord, S.; Sjöberg, B.; Mellander, O.; Hinton, M. Bronze-Type Structure of KNb_2O_5F and KTa_2O_5F. *Acta Chem. Scand.* **1965**, *19*, 1510−1510.
(25) Fourquet, J. L.; Jacoboni, C.; de Pape, R. Les Pyrochlores $A^IB_2X_6$: Mise en Evidence de L'occupation par le Cation A^I de Nouvelles Positions Cristallographiques Dans le Groupe D'Espace *Fd3m*. *Mater. Res. Bull.* **1973**, *8*, 393−403.
(26) Ming, H.; Zhang, J.; Liu, L.; Peng, J.; Du, F.; Ye, X.; Yang, Y.; Nie, H. A Novel Cs_2NbOF_5:Mn^{4+} Oxyfluoride Red Phosphor for Light-Emitting Diode Devices. *Dalton Transactions* **2018**, *47*, 16048−16056.
(27) De-Yu, L.; Lundberg, M.; Werner, P.; Westdahl, M. Occurence of the Tetragonal Tungsten Bronze Structure Type in the KF-Nb_2O_5 System. *Acta Chem. Scand.* **1984**, *38A*, 813−817.
(28) Vandenborre, M. T.; Husson, E.; Fourquet, J. L. Etude Spectroscopique Par Absorption Infra-Rouge et Diffusion Raman de Composes Oxyfluores de Structure Pyrochlore ANb_2O_5F (A = Rb, Cs, Tl) et $RbTa_2O_5F$. *Mater. Res. Bull.* **1982**, *17*, 1359−1364.
(29) Yoo, C.-Y.; Kim, J.; Kim, S.-C.; Kim, S.-J. Crystal Structures of New Layered Perovskite-Type Oxyfluorides, $CsANb_2O_6F$ (A = Sr and Ca) and Comparison with Pyrochlore-Type $CsNb_2O_5F$. *J. Solid State Chem.* **2018**, *267*, 146−152.
(30) Dissanayake, K. T.; Mendoza, L. M.; Martin, P. D.; Suescun, L.; Rabuffetti, F. A. Open-Framework Structures of Anhydrous Sr$(CF_3COO)_2$ and Ba$(CF_3COO)_2$. *Inorg. Chem.* **2016**, *55*, 170−176.
(31) Rietveld, H. Line Profiles of Neutron Powder-Diffraction Peaks for Structure Refinement. *Acta Crystallogr.* **1967**, *22*, 151−152.
(32) Rietveld, H. A Profile Refinement Method for Nuclear and Magnetic Structures. *J. Appl. Crystallogr.* **1969**, *2*, 65−71.
(33) Toby, B. H.; Von Dreele, R. B. GSAS-II: The Genesis of a Modern Open-Source All Purpose Crystallography Software Package. *J. Appl. Crystallogr.* **2013**, *46*, 544−549.
(34) Momma, K.; Izumi, F. VESTA 3 for Three-Dimensional Visualization of Crystal, Volumetric and Morphology Data. *J. Appl. Crystallogr.* **2011**, *44*, 1272−1276.
(35) Altomare, A.; Cuocci, C.; Giacovazzo, C.; Moliterni, A.; Rizzi, R.; Corriero, N.; Falcicchio, A. EXPO2013: A Kit of Tools for Phasing Crystal Structures from Powder Data. *J. Appl. Crystallogr.* **2013**, *46*, 1231−1235.
(36) Altomare, A.; Campi, G.; Cuocci, C.; Eriksson, L.; Giacovazzo, C.; Moliterni, A.; Rizzi, R.; Werner, P.-E. Advances in Powder Diffraction Pattern Indexing: N-TREOR09. *J. Appl. Crystallogr.* **2009**, *42*, 768−775.
(37) Boultif, A.; Louer, D. Powder Pattern Indexing with the Dichotomy Method. *J. Appl. Crystallogr.* **2004**, *37*, 724−731.
(38) Boultif, A.; Louer, D. Powder Pattern Indexing and the Dichotomy Algorithm. *Z. Kristallograph., Suppl.* **2007**, *26*, 191−196.
(39) Altomare, A.; Caliandro, R.; Camalli, M.; Cuocci, C.; da Silva, I.; Giacovazzo, C.; Moliterni, A. G. G.; Spagna, R. Space-Group Determination from Powder Diffraction Data: A Probabilistic Approach. *J. Appl. Crystallogr.* **2004**, *37*, 957−966.
(40) Altomare, A.; Camalli, M.; Cuocci, C.; Giacovazzo, C.; Moliterni, A. G. G.; Rizzi, R. Advances in Space-Group Determination From Powder Diffraction Data. *J. Appl. Crystallogr.* **2007**, *40*, 743−748.
(41) Le Bail, A.; Duroy, H.; Fourquet, J. L. Ab-Initio Structure Determination of $LiSbWO_6$ by X-ray Powder Diffraction. *Mater. Res. Bull.* **1988**, *23*, 447−452.
(42) McNulty, J. A.; Gibbs, A. S.; Lightfoot, P.; Morrison, F. D. Phase Transitions in the Hexagonal Tungsten Bronze $RbNbW_2O_9$. *J. Solid State Chem.* **2020**, *286*, 121275.
(43) Morniroli, J. P.; Steeds, J. W. Microdiffraction as a Tool for Crystal Structure Identification and Determination. *Ultramicroscopy* **1992**, *45*, 219−239.
(44) McNulty, J. A.; Tran, T. T.; Halasyamani, P. S.; McCartan, S. J.; MacLaren, I.; Gibbs, A. S.; Lim, F. J. Y.; Turner, P. W.; Gregg, J. M.; Lightfoot, P.; Morrison, F. D. An Electronically Driven Improper Ferroelectric: Tungsten Bronzes as Microstructural Analogs for the Hexagonal Manganites. *Adv. Mater.* **2019**, *31*, 1903620.
(45) Birchall, J. M.; Haszeldine, R. N.; Roberts, D. W. Cyclopropane Chemistry. Part II. Cyclopropanes as Sources of Difluorocarbene. *Journal of the Chemical Society, Perkin Transactions 1* **1973**, *0*, 1071−1078.
(46) Barela, M. J.; Anderson, H. M.; Oehrlein, G. S. Role of C_2F_4, CF_2, and Ions in C_4F_8/Ar Plasma Discharges Under Active Oxide Etch Conditions in an Inductively Coupled GEC Cell Reactor. *Journal of Vacuum Science & Technology A* **2005**, *23*, 408−416.
(47) Farjas, J.; Camps, J.; Roura, P.; Ricart, S.; Puig, T.; Obradors, X. The Thermal Decomposition of Barium Trifluoroacetate. *Thermochim. Acta* **2012**, *544*, 77−83.
(48) Mosiadz, M.; Juda, K. L.; Hopkins, S. C.; Soloducho, J.; Glowacki, B. A. An In-Depth in situ IR Study of the Thermal Decomposition of Yttrium Trifluoroacetate Hydrate. *J. Therm. Anal. Calorim.* **2012**, *107*, 681−691.
(49) Sävborg, Ö. Structures of Niobium and Tantalum Oxide Fluorides Containing Lone-Pair Ions: V. $Pb_xM(O,F)_{3+x/2}$ ($x \sim 0.25$, M = Nb, Ta): A Disordered Superstructure of the Hexagonal Tungsten Bronze Type. *J. Solid State Chem.* **1985**, *57*, 160−165.
(50) von Rohr, F. O.; Ryser, A.; Ji, H.; Stolze, K.; Tao, J.; Frick, J. J.; Patzke, G. R.; Cava, R. J. The *h*-Sb_xWO_{3+2x} Oxygen Excess Antimony Tungsten Bronze. *Chem. Eur. J.* **2019**, *25*, 2082−2088.
(51) Jin, L.; Guo, S.; Cava, R. J. $Sn_{0.24}WO_3$ Hexagonal Tungsten Bronze Prepared Via the Metal Chloride Route. *J. Solid State Chem.* **2020**, *291*, 121553.

https://doi.org/10.1021/acs.inorgchem.4c01700
Inorg. Chem. 2024, 63, 11842−11851